Contents lists available at SciVerse ScienceDirect

CIRP Annals Manufacturing Technology

Journal homepage: www.elsevier.com/locate/cirp

# Folding-shearing: shrinking and stretching sheet metal with no thickness change

Julian M Allwood[a] (1), Christopher J Cleaver[a], Evripides G Loukaides[b], Omer Music[c], Adam Nagy-Sochacki[a]

[a]*Department of Engineering, University of Cambridge, UK,* [b]*Department of Mechanical Engineering, University of Bath, UK,* [c]*Department of Mechanical Engineering, TED University, Ankara, Turkey.*

50% of all sheet metal is scrapped, mainly by trimming following deep-drawing. To combat this a novel process inspired by the mechanics of spinning is proposed and its feasibility is tested with a novel experimental rig. A sheet is first folded along its long axis and then drawn through a die-set in a state of shear to reduce its width with no average reduction of thickness. The performance and limits of the process are evaluated with a novel experimental rig and new analytical and numerical simulations. The extension from this pre-cursor process to a more general forming process is discussed.

Sheet metal, bending, shearing

## 1. Introduction

On average, the world's automotive manufacturers scrap half the sheet metal they purchase, mainly when trimming components after deep-drawing. This waste arises mainly from the use of material in the blank-holder and in "addendum surfaces" [1]. The material in the blank-holder is currently essential for managing the process window between wrinkling and tearing failures in deep-drawing. Might it be possible to form deep-drawn shapes without a blank-holder but at comparable speed?

Craft-workers have, for over 5000 years, used the manual processes of sinking and raising to form deep-drawn shapes without any material wastage [2]. Sinking, akin to incremental forming processes leads to thinning proportional to the depth of draw. This has been used for flanging, but the process is limited by thickness change [3]. By contrast, in raising, starting from a shallow curved dish, craftsmen incrementally form workpieces into deep shapes, by hammering over a smooth anvil or stake. Each stroke of the hammer falls just ahead of the contact with the stake stretching the workpiece away from the craftsman but working against the existing curvature of the dish to create circumferential compression. As a result, skilled workers can (with annealing where required) create extraordinarily deep geometries with no significant change of thickness in the sheet.

Spinning creates similar mechanics to those of raising, with the working roller pressing against existing curvature to create circumferential compression and radial tension, which when perfectly balanced, leads to shape change without thickness change [4]. Forming limit diagrams show an asymptote when the minor strain is equal to the negative of the major strain, indicating that this form of deformation gives the greatest potential for shape change [5]. Furthermore, forming in a state of pure shear-stress will minimize the hydrostatic pressure in the workpiece, and hence minimize tool forces and the work required to overcome friction. If all material elements also follow paths of proportional true strain (i.e. they experience only pure shear in the same direction) this meets the conditions of "ideal forming" [6].

A previous study [7] attempted to exploit the favourable mechanics of raising or spinning by a two-stage process of folding prior to pressing, but failed as the pressing stage largely reversed the folding. Figure 1 illustrates our new process concept [8], in which a shrink corner is formed in three stages, each of which comprises folding followed by shearing. In the shearing step, the curvature of the sheet at the corner resists a normal force applied by a sliding horseshoe-shaped die. This leads to circumferential compression and radial tension, exactly as occurs in the intermediate stages of metal-spinning. Unlike deep-drawing, the straight flange is deformed by pure bending and at the corner, no blank-holder is required to create the radial tension which counters the tendency of the sheet to wrinkle. If the tension and compression components of stress have equal magnitude, the deformation will be thickness neutral.

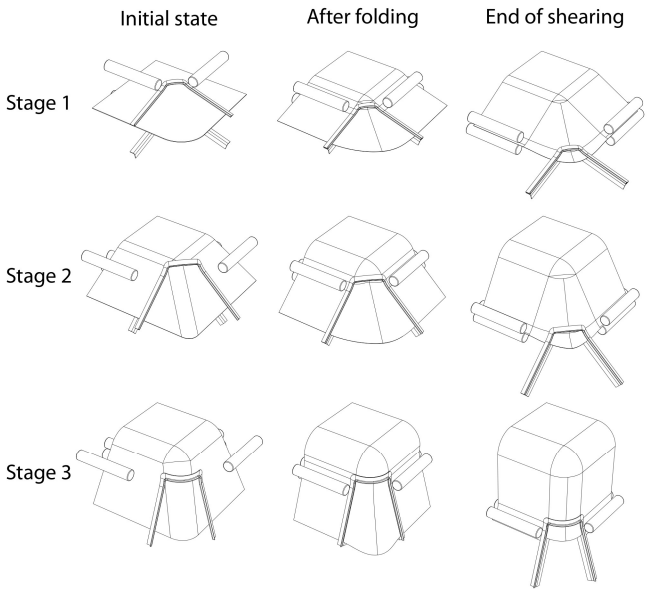


**Figure 1.** Novel process concept for folding-shearing a shrink corner

Prior to attempting a complete process design, this paper explores a pre-cursor process, representing only the corner of stage 1 in fig. 1 with folding followed by drawing through dies. This is where most plastic deformation would occur in the process of fig. 1, so if successful, will provide design parameters for trials with square cups. The idea has some similarity to draw-bending [9] but is different in aiming to change the width of the drawn workpiece.

## 2. Process concept

The test introduced in this paper is illustrated in fig. 2. A strip of metal is folded along its long axis and then drawn at an angle and under tension through a die. The reaction force of the die pressing against the workpiece creates compression perpendicular to the direction of travel, so that the workpiece is once-again flat as it leaves the die, but with reduced width and no thickness change. The folding half-angle $\alpha$ determines the width-change and the angle of attack $\theta$ controls the ratio between exit tension and the die force.

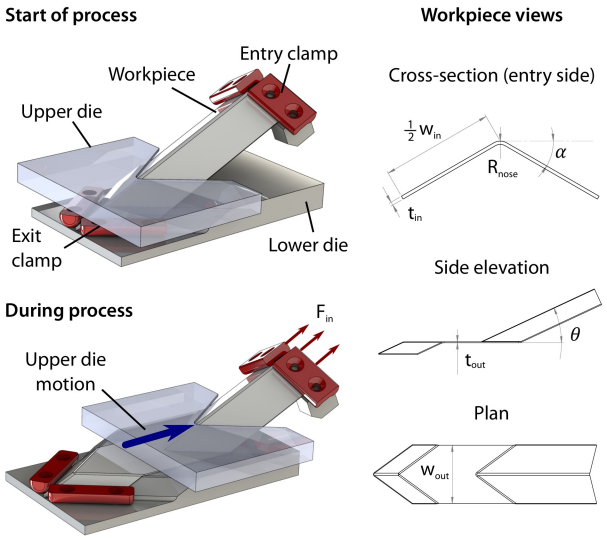


**Figure 2.** Pre-cursor process concept for folding-shearing sheet metal

If the streamlines of material flow through the process remain at constant separation when seen in plan-view, then using $w$ (width), $t$ (thickness), $v$ (velocity), the process will lead to the outcomes:

$$\frac{w_{out}}{w_{in}} = \cos\alpha\,,\ t_{out} = t_{in},\ \frac{v_{in}}{v_{out}} = \frac{w_{out}}{w_{in}},\ \bar{\epsilon} = \frac{2}{\sqrt{3}}(1-\cos\alpha) \qquad (1)$$

The input parameters for the process are the sheet's initial thickness and width, the two angles $\alpha$ and $\theta$, material and friction parameters and the entry tension. The process outputs are the exit tension, distributions across the output width of thickness, residual stress and hardness, and any process failures or damage.

## 3. Experimental design

A novel experimental rig has been designed to test the process. The rig has exchangeable dies and uses a manual handwheel to move the upper die relative to the sample which is clamped to a fixed lower die on its exit side. A hydraulic actuator is used to control the entry tension via a clamp attached to the sheet on its entry edge. The clamps at the two ends of the strip are far enough from the area of deformation to have only a scalar influence on the plastic stress state. The experimental rig was specified to process strips of Al 1050-H14 with exit width 60mm and entry thickness 0.9mm.

A campaign of experimental trials was conducted on the rig as specified in table 1. The tensile force $F_{in}$, applied to the entering material, is reported relative to $F_y$, the force required to cause uniaxial yielding. Following the trials, the exit strip width change, thickness distribution and hardness were measured.

**Table 1.** Parameter settings for trials conducted on the rig.

| $R_{nose}$ | α | θ | $F_{in}/F_y$ |
|---|---|---|---|
| 4mm | 30°, 45° | 20°, 25°, 30° | 0, 5%, 25%, 50% |

## 4. Simulation

A finite element simulation was created in Abaqus Implicit, using elements of type S4R for the workpiece and R3D4 for the dies (with approx. size 2 and 1.6mm respectively), a "hard" contact model and frictionless conditions. The clamps at strip ends were represented as displacement constraints, with an edge load imposing tension on one end. The simulation was validated by comparing the exit thickness distribution between experiments and simulations, as shown in fig. 3. The results suggest that the simulation outputs, while not perfect, are indicative of real process behaviour.

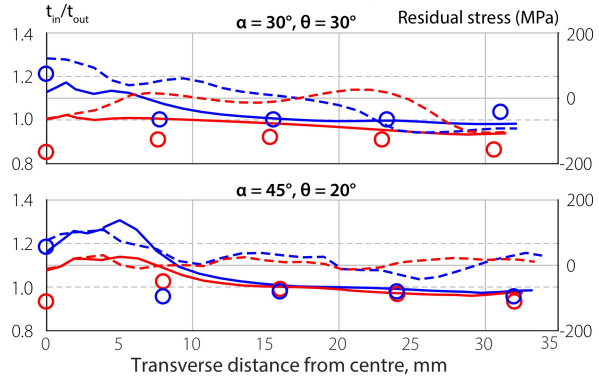


**Figure 3.** Thickness and residual stress distributions (blue: $F_{in}$=0; red: $F_{in}$=0.5$F_y$; solid lines: simulated thickness; dashed lines simulated residual stress; circles: measured thickness.)

The thickness variation leads to some residual stress also shown in fig. 3 and the distributions in fig. 4 of equivalent strain and hardness (measured by a Shimadzu micro hardness tester, test weight 2.942N, with tests taken at midpoint through the sheet thickness.) The results of fig. 3 show a small increase in thickness in the centre of the sheet, which arises from the small nose radius used in these trials. Near the fold, thickening has occurred leading to an increased equivalent strain. This effect is more pronounced for the higher fold angle, $\alpha = 45°$. In the three-stage process of fig. 1 this effect will influence the responses of stages 2 and 3, and may allow a useful control of thickness variation in the final product. The simulation was used to explore the wider range of process conditions in table 2.

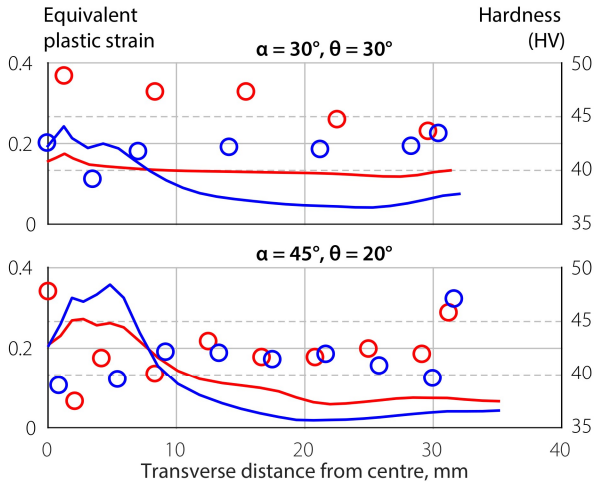


**Figure 4.** Comparison of simulated strain and measured hardness (blue: $F_{in}$=0; red: $F_{in}$=0.5$F_y$; lines: simulated strain; circles: measured hardness.)

**Table 2.** Parameter settings for trials conducted by simulation.

| $R_{nose}$ | α | θ | $F_{in}/F_y$ |
|---|---|---|---|
| 4mm | 22.5°, 30°, 37.5°, 45° | 20°, 25°, 30° | 0, 5%, 25%, 50% |
| 10mm | 22.5°, 30°, 37.5°, 45° | 20°, 25°, 30° | 25% |
| 20mm | 22.5°, 30°, 37.5°, 45° | 20°, 25°, 30° | 25% |
| 30mm | 22.5°, 30°, 37.5°, 45° | 20°, 25°, 30° | 25% |

## 5. Results and process assessment

Figure 5 shows the outcomes of the physical trials. For the more aggressive trials (with $\alpha$ =45° and hence by eqn. (1) an attempted width-reduction of 29%) only the highest entry tension and lowest angle of attack $\theta$ =20° completed successfully. Even in this trial, some evidence of incipient failure at the nose is apparent. However, all of the trials with folding half-angle $\alpha$ =30° (width-reduction 13%) completed successfully, even when no entry tension was applied. This result guided the selection of the range of folding angles specified in the simulation trials listed in table 2.

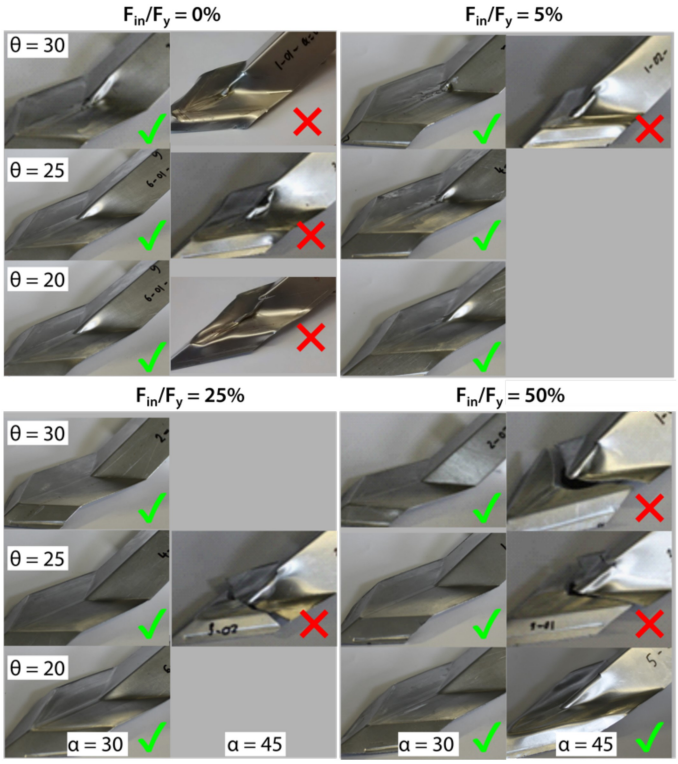


**Figure 5.** Summary of experimental results showing success and failure.

Although, implicit FEA is generally not reliable for capturing wrinkling, both simulation and experiments indicate that the most common process failure is the instability of the form shown in fig. 6: as soon as die motion begins, the workpiece folds to a tighter angle than that of the die. Soon, this creates a crease which leads to thickening at the fold. If the process is not stopped, this thickening causes the workpiece to 'lock' between upper and lower die.

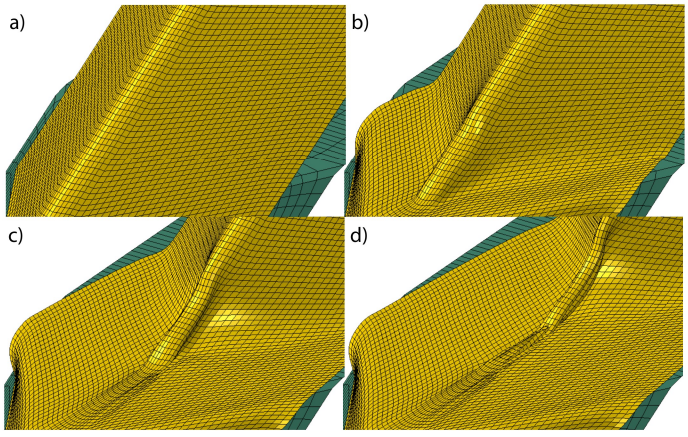


**Figure 6.** Progression of process instability in FE for α=45°, θ = 30°, $F_{in}$ = 0.

Figure 7 shows the width reduction for different values of entry tension. According to eqn. (1) this should depend only on $\alpha$, but the results deviate from this ideal. However, the predicted changes show closer agreement at higher $\theta$. In both experiments and simulation, the edges of the workpiece are free, so at lower angles of attack $\theta$ (with correspondingly reduced exit tension) some material "un-folds" as it passes through the die. As the angle of attack increases, the geometry of the die and exit tension provide an increasing restraint and so maintain more parallel streamlines.

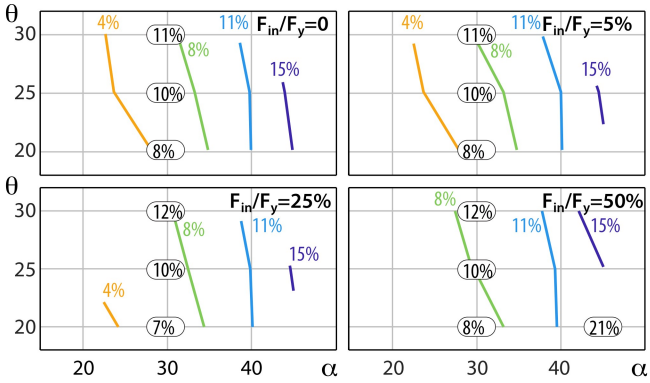


**Figure 7.** Width reduction for varying tension, $F_{in}/F_y$, fold half-angle, α and angle of attack, θ: experiment (ellipses) and FE (contours)

Figure 7 shows that the entry tension has little impact on width change. For $\alpha$ = 30°, eqn. (1) predicts a width reduction of 13%, and the experimental results tend towards this with increasing $\theta$. However, fig. 8 shows that increasing the nose radius of the fold reduces the predicted width reduction, and at lower angles of attack, very little change is achieved, even with high fold-angles.

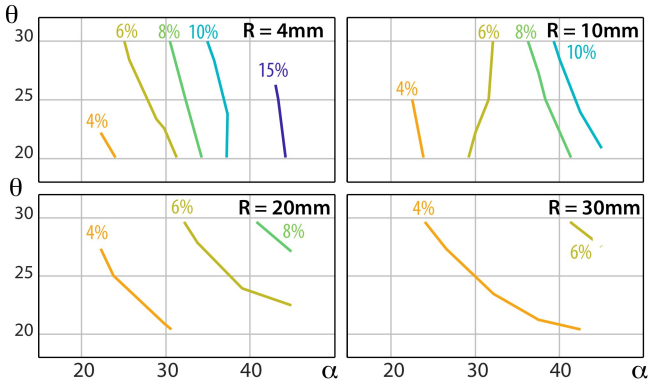


**Figure 8**. Width reduction for varying fold radius, R, fold half-angle, α and angle of attack, θ with $F_{in}/F_y$ = 25%

Figure 9 extends fig. 3 to show that increasing the nose radius leads to more uniform thickness, as the larger radius creates less restraint on un-folding, so leads to less width reduction.

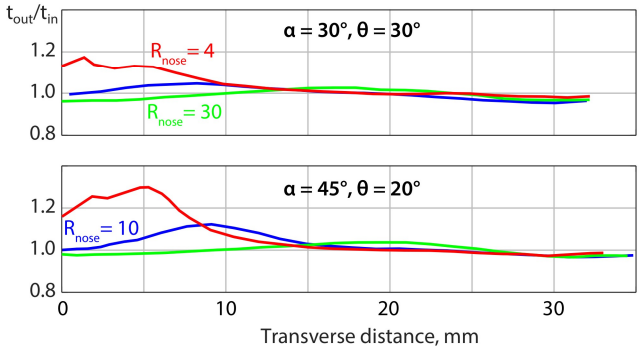


**Figure 9.** Simulated effect of fold nose-radius on thickness distribution

To explore this further, figs. 10 & 11 demonstrate the maximum increase in thickness over the same range of input parameters tested in figs. 7 & 8.

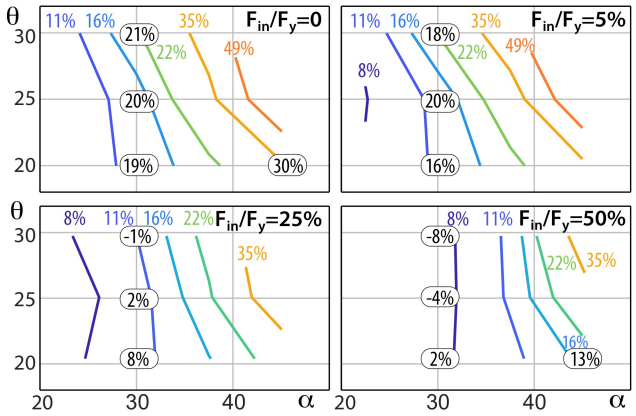


**Figure 10.** Maximum thickening for varying tension, $F_{in}/F_y$, fold half-angle, α and angle of attack, θ with $R_{nose}$ = 4 mm: experiment (quoted values) vs FE (contours)

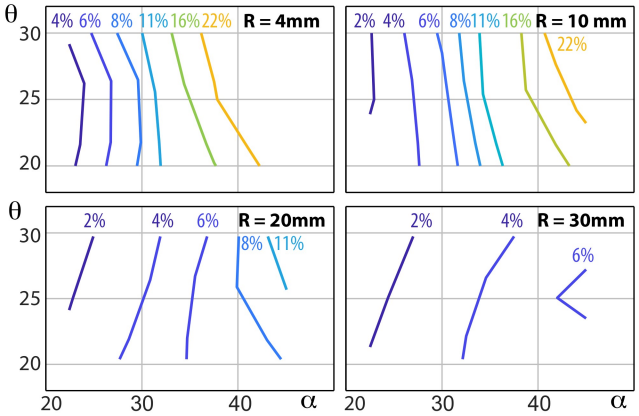


**Figure 11.** Simulated maximum thickening for varying fold radius, R, fold half-angle, α and angle of attack, θ

Figure 10 demonstrates that some entry tension is essential to controlling thickening. The fold angle influences maximum thickening significantly more than the angle of attack in both the simulated and measured results. Figure 11 predicts a very strong influence of nose radius on maximum thickening – albeit this also relates to the limited width change illustrated in fig. 8 for larger radii.

Overall, the results of experimental and simulated trials on the novel pre-cursor process suggest that folding and shearing can change the width of a sample without significant thickness change. In the set up used here, with free edges to the sample, the greatest width change occurs with high fold angles, and the thickness distribution is best controlled with high nose radii.

Figure 12 uses the simulation to reveal the strain history of the process, plotted on the axes of a forming limit diagram. As anticipated in the motivation for the process, the strain state is close to pure shear, although in this case study with high entry tension, some thinning is apparent at the strip edge.

## 6. Discussion and conclusions

The novel process described in this paper has demonstrated that the favourable mechanics observed in spinning and raising processes can be re-created in a more continuous form of deformation: working against prior curvature, it is possible to create large shape changes without changing the thickness of the workpiece.

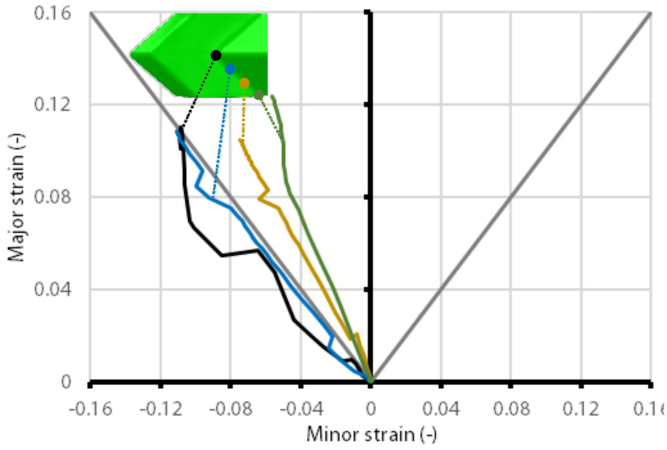


**Figure 12.** Strains created by the process plotted on FLD axes - 4 points across half width, for α = 30, θ = 30 and $F_{in}/F_y$ = 50%

The degree of shape change can be controlled and based on the results of the paper, fig. 13 anticipates an operating window for the process. Higher tensile forces applied to the entering material increase the amount of width change possible before process instability. Increasing the nose radius reduces the resulting variation in thickness at the cost of reduced width reduction.

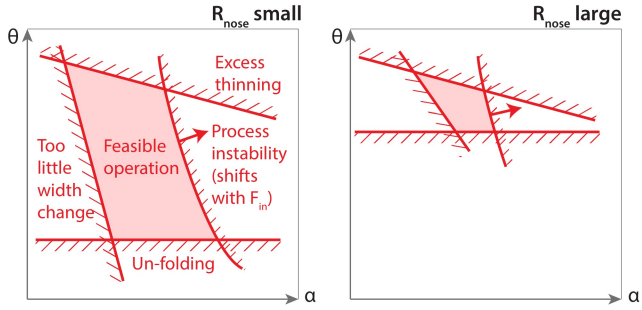


**Figure 13**. Conceptual operating window for the process

The novel process introduced in this paper leads to nearly pure shear, with high surface quality, and allows width reductions of 10-15% per pass across a range of operating conditions. Further experimental trials will allow confirmation of the predicted effects of varying the nose radius, but the results give confidence that the more practical process illustrated in fig. 1 is achievable, and the estimated operating window provides guidance for its realisation.

## Acknowledgements

The work of Professor Allwood and Dr Cleaver on this project was funded by EPSRC grant EP/K018108/1.

## References

[1] Horton, P.M. and Allwood, J.M., 2017. Yield improvement opportunities for manufacturing automotive sheet metal components. J Mat. Proc. Tech., 249, 78-88.
[2] Holtzapffel, C., 1852. Turning and Mechanical Manipulation: Intended as a Work of General Reference and Practical Instruction, on the Lathe, and the Various Mechanical Pursuits Followed by Amateurs (Vol. 1).
[3] Voswinckel, H., Bambach, M. and Hirt, G., 2015. Improving geometrical accuracy for flanging by incremental sheet metal forming. I J Material Forming, 8(3), 391-399.
[4] Music, O., Allwood, J.M. and Kawai, K., 2010. A review of the mechanics of metal spinning. Journal of materials processing technology, 210(1), pp.3-23.
[5] Allwood, J.M. and Shouler, D.R., 2009. Generalised forming limit diagrams showing increased forming limits with non-planar stress states. I J Plasticity, 25(7), 1207-1230.
[6] Richmond, O. and Chung, K., 2000. Ideal stretch forming for minimum weight axisymmetric shell structures. I J mechanical sciences, 42(12), pp.2455-2468.
[7] Carruth, M.A. and Allwood, J.M., 2013. A novel process for transforming sheet metal blanks: Ridged die forming. CIRP Annals, 62(1), pp.267-270.
[8] Allwood, J.M., Cleaver, C.J., Nagy, A., Music, O. and Loukaides, E (2018) Working of sheet metal. Patent application, Ref GB1814069.9.
[9] Behrens, B.A., Rosenberger, J., Süße, D. and Ulbricht, V., 2009. Cost-efficient fabrication of load-adapted profiles by draw bending. I J Material Forming, 2(1), p.785.